



HAL
open science

Distributed transfer function-based unified static solutions for piezoelectric short/open-circuit sensing and voltage/charge actuation of beam cantilevers

Majed Majeed, Aych Benjeddou, Mohammed Al-Ajmi

► To cite this version:

Majed Majeed, Aych Benjeddou, Mohammed Al-Ajmi. Distributed transfer function-based unified static solutions for piezoelectric short/open-circuit sensing and voltage/charge actuation of beam cantilevers. *Acta Mechanica*, 2021, 232 (3), pp.1025-1044. 10.1007/s00707-020-02867-5 . hal-03239768

HAL Id: hal-03239768

<https://hal.science/hal-03239768>

Submitted on 1 Sep 2022

HAL is a multi-disciplinary open access archive for the deposit and dissemination of scientific research documents, whether they are published or not. The documents may come from teaching and research institutions in France or abroad, or from public or private research centers.

L'archive ouverte pluridisciplinaire **HAL**, est destinée au dépôt et à la diffusion de documents scientifiques de niveau recherche, publiés ou non, émanant des établissements d'enseignement et de recherche français ou étrangers, des laboratoires publics ou privés.



Distributed under a Creative Commons Attribution - NonCommercial 4.0 International License

Distributed transfer function-based unified static solutions for piezoelectric short/open-circuit sensing and voltage/charge actuation of beam cantilevers

Majed A. Majeed, Ayech Benjeddou, Mohammed Al-Ajmi

Abstract Closed-form unified solutions using the distributed transfer functions (DTFs) method are presented for the first time for the static short/open-circuit sensing and voltage/charge actuation of moderately thick beam cantilevers with co-localized surface-bonded piezoelectric patches. For this purpose, the smart beam is divided into three segments, of which the clamp and free sides parts are elastic, while the middle one is made of an elastic core sandwiched between two electroded piezoelectric patches. The latter can be different in material properties and thickness but should have the same length, and their widths can be different from the host elastic beam. The theoretical formulation is based on Timoshenko's first-order shear deformation theory for the kinematics and piezoelectric constitutive equations and the principle of virtual works for the variational equations. The latter integrate explicitly the physical equipotential constraints on the patches electrodes. The balance equations and boundary conditions are derived for the three segments independently and then connected at their interfaces by the equilibrium equations and continuity conditions. The unified static solutions for the resulting four problems are derived analytically in closed form using the DTF approach. These are validated against only open literature benchmarks having tabulated results or analytical formulas in order to avoid curves induced inherent additional deviations. Very good correlations were obtained in comparison with the found reference two-dimensional (2D) plane strain/stress analytical and 2D plane strain/stress and three-dimensional finite element results.

1 Introduction

Piezoelectric unimorph and trimorph (bimorph with elastic core) cantilevers find wide use in smart structures applications. This is the case in vibration energy harvesting [1] and shunted damping [2], while beam cantilevers with surface-mounted piezoelectric patches are common for structural active vibration control [3]. One-dimensional (1D) or two-dimensional (2D) models of such smart beams are reduced from three-dimensional (3D) ones after various first- or higher-order electromechanical assumptions [4]. They differ by the retained distributions of the mechanical displacements and transverse shear stress or strain and the electric potential and the reduced constitutive equations. Various methods can be used for solving the corresponding electromechanical partial derivative equations (PDE). This includes analytical closed-form solutions (CFS), semi-analytical

M. Majeed (✉) · M. Alajmi
Mechanical Engineering Department, Kuwait University, P.O. Box 5969, 13060 Safat, Kuwait
E-mail: m.majeed@ku.edu.kw

A. Benjeddou
ROBERVAL FRE 2012 UTC/CNRS, Rue Personne de Roberval, 60200 Compiègne, France

A. Benjeddou
Institut Supérieur de Mécanique de Paris, 3 rue Fernand Hainaut, 93400 Saint Ouen, France

state space methods (SSM), among which is the distributed transfer function (DTF) approach, and finite element methods (FEM) [3]. The latter are usually validated using either of the former. These can be also used for parametric analysis in the aim of understanding coupling effects or optimization for performance maximization.

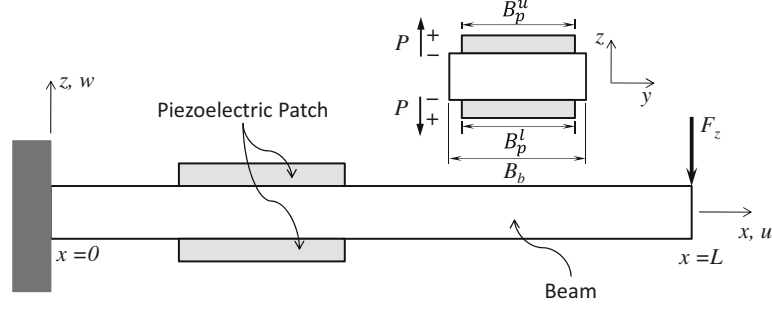
The DTF approach used in modeling elastic beam cantilevers dates back to the early nineties [5] but only to the last decade for piezoelectric ones, as reviewed in [6]. It was often used for solving dynamic problems, particularly for vibration analysis [7]. In the latter two works [6,7], the smart beam cantilever, with different piezoelectric surface-bonded patches and having different thickness than the host was divided into three segments, representing the cantilevered (segment 1), smart (segment 2), and free (segment 3) parts. For each of the latter, the PDE was derived using Timoshenko's first-order shear deformation theory (FSDT), along with the plane-stress reduced constitutive equations as given in [8], from the principle of Hamilton extended to piezoelectricity [9], then connected by the inter-segments continuity conditions (CCs) and balance equations or boundary conditions (BCs). The DTF was then used for deriving the eigenvalue problems under short-circuit (SC) and open-circuit (OC) electrodes fulfilling automatically the equipotential (EP) physical constraints.

It is worth noticing that, from the above literature reviews, the different patches and beam widths and EP constraints were not considered simultaneously. Besides, the DTF approach was not used for the static sensing and actuation of elastic beam cantilevers with surface-bonded piezoelectric patches or layers. It is then the objective of the present work to extend the authors' earlier works on vibration analysis of asymmetric [6] and symmetric [7] beam cantilevers to their static voltage or charge actuation and SC or OC sensing. Also, only two references [10,11] were found about charge actuation [10] and sensing [11] of piezoelectric trimorphs; they will be then used for the validation of the corresponding DTF CFS. Similarly, for OC sensing with a single piezoelectric patch, fulfilling the EP physical constraints, only one reference [12] was found in the open literature; it is also used as a validation benchmark for the corresponding DTF CFS. However, no reference was found in the open literature about realistic (practical) configurations of beam cantilevers with different widths of patches and host. Thus, only benchmarks with same widths [10–14] will be used for validating the DTF CFS.

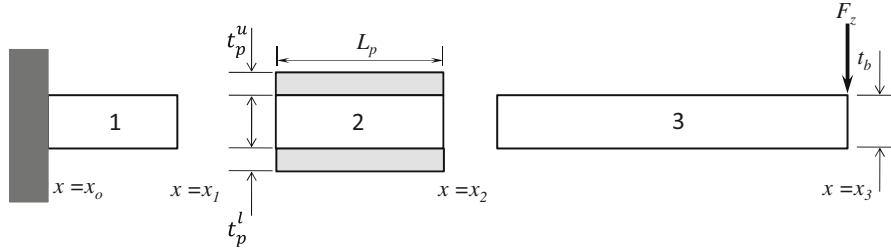
Therefore, in the following, the DTF-based static unified solutions for piezoelectric SC/OC sensing and voltage/charge actuation of beam cantilevers are presented. For this purpose, the three segments equilibrium local PDE, BC and inter-segments CC of a cantilever elastic beam, having two different piezoelectric patches on its top and bottom and with different width from that of the host, are first derived from their corresponding variational equations based on Timoshenko's FSDT of beams, but using the principle of virtual work (PVW), extended to piezoelectricity [9], and various FSDT-compatible 1D reductions of the 3D constitutive equations, including that proposed in [8] and used earlier in [6,7] and [12]. Then, the static sensing and actuation problems are derived using the DTF approach for voltage and charge inputs (actuation) and outputs (sensing). Next, in order to avoid inherent additional errors from comparisons to graphical results, the presented CFS are validated only against available tabulated results [10–12,14] or analytical formulas [13] in the open literature. Finally, some conclusions and perspectives of the present work are provided as a closure.

2 Piezoelectric beam cantilevers problem formulation

The considered piezoelectric smart beam cantilever and its decomposition into three segments, where the extreme ones (1,3) are for the bare parts and the middle one (2) is for the sandwich part made of an elastic core and piezoelectric skins, are shown in Fig. 1. The beam lies in the x - z plane, where the x -axis is along the length and the z -axis is in the thickness direction (upward). The coordinates originate at the intersection of the beam's clamped edge and reference mid-plane. The beam is of length $L = x_3 - x_0$, where x_0 and x_3 are the abscissa of the clamp and free edge. It is of width B_b , thickness t_b and elastic orthotropic behavior with material axes (1, 2, 3) coinciding with the Cartesian coordinate system ones (x, y, z). The surface-bonded patches have outward opposite polarizations along the thickness and a 2-mm crystal class piezoelectric behavior. They can be different in material properties, thickness t_p and width B_p , where u and l superscripts will be used for specifying the characteristics of the upper and lower patches. However, the latter have the same length $L_p = x_2 - x_1$, where x_1 and x_2 are the positions (from the clamp) of their left and right edges. They can be actuated by applied voltage V or charge Q , and both can be sensed when the beam's tip is subjected to a downward concentrated force, F_z . Note that when grounding the patches interfaces with the beam, the upper V^u and lower V^l voltages are, respectively, positive and negative, see Fig. 1a.



(a) Coordinate system and poling directions



(b) Segmented configuration

Fig. 1 Cantilever beam with two co-localized surface-mounted piezoelectric patches

2.1 Kinematics and constitutive equations

The cantilever smart piezoelectric beam is supposed moderately thick and can be modeled using Timoshenko's FSDT. Thus, the axial u and transverse w global displacements can be written in terms of the mid-plane axial u_o , transverse w_o and bending rotation ψ generalized displacements

$$u(x, z) = u_o(x) + z\psi(x), \quad w(x, z) = w_o(x). \quad (1)$$

Consequently, the linearized strain–displacement relations reduce to these axial and transverse shear (TS) strain–generalized displacement relations,

$$\varepsilon_x = u_o' + z\psi', \quad \gamma_{xz} = \psi + w_o', \quad (2)$$

where the prime $(.)'$ denotes the derivative with respect to the spatial coordinate x .

As the piezoelectric patches are electroded and thin, it can be reasonably assumed that the transverse electric field component, E_z , dominates the in-plane ones and can be written in terms of the voltage and patch thickness so that $E_z = -V/t_p$. In this case, the axial and TS stresses, dual to the above strains, are functions of the latter and the dominant electric field so that the 3D converse piezoelectric constitutive equations for a thickness polarization reduce to

$$\begin{Bmatrix} \sigma_x \\ \tau_{xz} \end{Bmatrix} = \begin{bmatrix} \tilde{Q}_{11}^E & 0 \\ 0 & k_s \tilde{Q}_{55}^E \end{bmatrix} \begin{Bmatrix} \varepsilon_x \\ \gamma_{xz} \end{Bmatrix} - \begin{Bmatrix} \tilde{e}_{31} \\ 0 \end{Bmatrix} E_z \quad (3)$$

where k_s is the classical shear correction factor taken here equal to 5/6 [8], and \tilde{Q}_{11}^E , \tilde{Q}_{55}^E and \tilde{e}_{31} are, respectively, the axial and TS stiffness (under constant electric field) and stress piezoelectric coefficients, modified or not depending on the considered 3D to 1D constitutive equations reduction.

Notice that Eq. (3) is a general form compatible with the FSDT so that any expressions for its stiffness and stress piezoelectric coefficients can be used in the hereafter proposed theoretical formulation and DTF CFS. These coefficients are usually taken as those derived in [8] and used in [6,7,12], i.e.,

$$\tilde{Q}_{11}^E = C_{11}^E - C_{13}^E \frac{C_{13}^E}{C_{33}^E}, \quad \tilde{Q}_{55}^E = C_{55}^E, \quad \tilde{e}_{31} = e_{31} - e_{33} \frac{C_{13}^E}{C_{33}^E} \quad (4)$$

where C_{11}^E , C_{13}^E , C_{33}^E , and C_{55}^E are the 3D elastic stiffness coefficients at constant electric field and e_{31} and e_{33} are the 3D stress piezoelectric coefficients.

The constitutive Eq. (3) is useful for actuation, while for sensing the 3D direct piezoelectric constitutive equation is reduced to this expression of the dielectric transverse displacement component, D_z , dual to the dominant electric field one, E_z ,

$$D_z = \tilde{e}_{31} \varepsilon_x + \tilde{\epsilon}_{33}^S E_z, \quad (5)$$

where $\tilde{\epsilon}_{33}^S$ is the modified or not dielectric coefficient (at constant strain), which expression depends also on the retained 3D-to-1D constitutive equations reduction.

It is worth noticing that Eq. (5) is a general form compatible with the FSDT so that any expression for its dielectric coefficient at constant strain can be used in the hereafter proposed theoretical formulation and DTF CFS. This coefficient is usually taken as that derived in [8] and used already in [6,7,12], i.e.,

$$\tilde{\epsilon}_{33}^S = \epsilon_{33}^S + e_{33} \frac{e_{33}}{C_{33}^E} \quad (6)$$

where ϵ_{33}^S is the 3D transverse dielectric coefficient at constant strain.

2.2 Variational equations

For kinematically admissible independent virtual variables (mechanical generalized displacements and electric potential), the PVW extended to piezoelectricity can be reduced to [9]

$$-\delta H + \delta W = 0 \quad (7)$$

where δH and δW are, respectively, the virtual electromechanical enthalpy and virtual works done by external electrical and mechanical loads.

For an FSDT-based piezoelectric beam, the virtual electromechanical enthalpy is written as [8]

$$\delta H = \int_{\Omega} (\delta \varepsilon_x \sigma_x + \delta \gamma_{xz} \tau_{xz} - \delta E_z D_z) d\Omega \quad (8)$$

where the integral on the volume Ω is separated into thickness, width and length single integrals in order to handle separately the smart beam cantilever's three segments. Thus, considering the latter, the integral along the beam length can be decomposed as

$$\int_0^L (\cdot) dx = \int_0^{x_1} (\cdot) dx + \int_{x_1}^{x_2} (\cdot) dx + \int_{x_2}^L (\cdot) dx. \quad (9)$$

Substituting the axial and shear strains and stresses, Eqs. (2) and (3), along with the electric displacement, Eq. (5), in Eqs. (8) and (9) and carrying out the width and through-the-thickness integrals, taking into consideration different beam and piezoelectric patches widths and thicknesses, results in the following

$$\delta H = B_p^u \int_{x_1}^{x_2} \left\{ \int_{\frac{t_b}{2}}^{\frac{t_b}{2} + t_p^u} \left[(\delta u'_o + z \delta \psi') (\tilde{Q}_{11}^{pu} u'_o + z \tilde{Q}_{11}^{pu} \psi' - \tilde{e}_{31}^u E_z^u) + (\delta \psi + \delta w'_o) k_s \tilde{Q}_{55}^{pu} (\psi + w'_o) \right. \right. \\ \left. \left. - \delta E_z^u (\tilde{e}_{31}^u u'_o + z \tilde{e}_{31}^u \psi' + \tilde{\epsilon}_{33}^{Su} E_z^u) \right] dz \right\} dx + B_p^l \int_{x_1}^{x_2} \left\{ \int_{\frac{-t_b}{2} - t_p^l}^{-\frac{t_b}{2}} \left[(\delta u'_o + z \delta \psi') (\tilde{Q}_{11}^{pl} u'_o + z \tilde{Q}_{11}^{pl} \psi' - \tilde{e}_{31}^l E_z^l) \right. \right. \\ \left. \left. - \delta E_z^l (\tilde{e}_{31}^l u'_o + z \tilde{e}_{31}^l \psi' + \tilde{\epsilon}_{33}^{Sl} E_z^l) \right] dz \right\} dx$$

$$\begin{aligned}
& + (\delta\psi + \delta w'_o) k_s \tilde{Q}_{55}^{pl} (\psi + w'_o) - \delta E_z^l (\tilde{e}_{31}^l u'_o + z \tilde{e}_{31}^l \psi' + \tilde{\epsilon}_{33}^{Sl} E_z^l) \Big] dz \Big\} dx, \\
& + B_b \int_0^L \left\{ \int_{-\frac{t_b}{2}}^{\frac{t_b}{2}} \left[(\delta u'_o + z \delta \psi') (\tilde{Q}_{11}^b u'_o + z \tilde{Q}_{11}^b \psi') + (\delta\psi + \delta w'_o) k_s \tilde{Q}_{55}^b (\psi + w'_o) \right] dz \right\} dx. \quad (10)
\end{aligned}$$

Note that since the reference plane is taken as the beam's mid-plane, the membrane-bending strains coupling terms in the first product of the third integral of Eq. (10) vanish automatically. It should also be noted that the first two thickness integrals in the above expression are only present in segment 2. Carrying out these through-the-thickness integrations results in the following expression for the virtual enthalpy:

$$\begin{aligned}
\delta H = & \int_{x_1}^{x_2} \left[A_p^u \delta u'_o (\tilde{Q}_{11}^{pu} u'_o + H_2^u \tilde{Q}_{11}^{pu} \psi' - \tilde{e}_{31}^u E_z^u) + \delta \psi' (A_p^u H_2^u \tilde{Q}_{11}^{pu} u'_o + I_p^u \tilde{Q}_{11}^{pu} \psi' - A_p^u H_2^u \tilde{e}_{31}^u E_z^u) \right. \\
& + (\delta\psi + \delta w'_o) k_s A_p^u \tilde{Q}_{55}^{pu} (\psi + w'_o) - \delta E_z^u (A_p^u \tilde{e}_{31}^u u'_o + A_p^u H_2^u \tilde{e}_{31}^u \psi' + A_p^u \tilde{\epsilon}_{33}^{Su} E_z^u) \Big] \\
& + \left[A_p^l \delta u'_o (\tilde{Q}_{11}^{pl} u'_o - H_2^l \tilde{Q}_{11}^{pl} \psi' - \tilde{e}_{31}^l E_z^l) - \delta \psi' (A_p^l H_2^l \tilde{Q}_{11}^{pl} u'_o - I_p^l \tilde{Q}_{11}^{pl} \psi' - A_p^l H_2^l \tilde{e}_{31}^l E_z^l) \right. \\
& + (\delta\psi + \delta w'_o) k_s A_p^l \tilde{Q}_{55}^{pl} (\psi + w'_o) - \delta E_z^l (A_p^l \tilde{e}_{31}^l u'_o - A_p^l H_2^l \tilde{e}_{31}^l \psi' + A_p^l \tilde{\epsilon}_{33}^{Sl} E_z^l) \Big] dx \\
& + \int_0^L \left[\delta u'_o A_b \tilde{Q}_{11}^b u'_o + \delta \psi' I_b \tilde{Q}_{11}^b \psi' + (\delta\psi + \delta w'_o) k_s A_b \tilde{Q}_{55}^b (\psi + w'_o) \right] dx \quad (11)
\end{aligned}$$

with $A_b = B_b t_b$, $A_p^u = B_p^u t_p^u$ and $A_p^l = B_p^l t_p^l$ being the cross-sectional areas of the beam and the upper and lower piezoelectric patches, respectively. I_b is the cross-section quadratic moment of the beam, and I_p^u and I_p^l are the cross-section quadratic moments of the upper and lower piezoelectric patches. These are defined as

$$I_b = \frac{B_b t_b^3}{12}, \quad I_p^u = \frac{t_p^u B_p^u}{12} \left[(t_p^u)^2 + 3(t_b + t_p^u)^2 \right], \quad I_p^l = \frac{t_p^l B_p^l}{12} \left[(t_p^l)^2 + 3(t_b + t_p^l)^2 \right]. \quad (12)$$

Note that the quantities H_2^u and H_2^l in Eq. (11) are defined as

$$H_2^u = \frac{1}{2}(t_b + t_p^u), \quad H_2^l = \frac{1}{2}(t_b + t_p^l). \quad (13)$$

Expanding the integration over the beam length and collecting terms with common integration limits yields

$$\begin{aligned}
\delta H = & \int_0^{x_1} \left[\delta u'_o A_b \tilde{Q}_{11}^b u'_o + \delta \psi' I_b \tilde{Q}_{11}^b \psi' + (\delta\psi + \delta w'_o) k_s A_b \tilde{Q}_{55}^b (\psi + w'_o) \right] dx \\
& + \int_{x_1}^{x_2} \left\{ \delta u'_o \left[(A_b \tilde{Q}_{11}^b + A_p^u \tilde{Q}_{11}^{pu} + A_p^l \tilde{Q}_{11}^{pl}) u'_o + (H_2^u \tilde{Q}_{11}^{pu} A_p^u - H_2^l \tilde{Q}_{11}^{pl} A_p^l) \psi' - (\tilde{e}_{31}^u A_p^u E_z^u + \tilde{e}_{31}^l A_p^l E_z^l) \right] \right. \\
& + \delta \psi' \left[(A_p^u H_2^u \tilde{Q}_{11}^{pu} - A_p^l H_2^l \tilde{Q}_{11}^{pl}) u'_o + (I_b \tilde{Q}_{11}^b + I_p^u \tilde{Q}_{11}^{pu} + I_p^l \tilde{Q}_{11}^{pl}) \psi' - (A_p^u H_2^u \tilde{e}_{31}^u E_z^u - A_p^l H_2^l \tilde{e}_{31}^l E_z^l) \right] \\
& + (\delta\psi + \delta w'_o) k_s (A_b \tilde{Q}_{55}^b + A_p^u \tilde{Q}_{55}^{pu} + A_p^l \tilde{Q}_{55}^{pl}) (\psi + w'_o) - \delta E_z^u (A_p^u \tilde{e}_{31}^u u'_o + A_p^u H_2^u \tilde{e}_{31}^u \psi' + A_p^u \tilde{\epsilon}_{33}^{Su} E_z^u) \\
& \left. - \delta E_z^l (A_p^l \tilde{e}_{31}^l u'_o - A_p^l H_2^l \tilde{e}_{31}^l \psi' + A_p^l \tilde{\epsilon}_{33}^{Sl} E_z^l) \right\} dx + \int_{x_2}^L \left[\delta u'_o A_b \tilde{Q}_{11}^b u'_o + \delta \psi' I_b \tilde{Q}_{11}^b \psi' + (\delta\psi + \delta w'_o) \right. \\
& \left. k_s A_b \tilde{Q}_{55}^b (\psi + w'_o) \right] dx. \quad (14)
\end{aligned}$$

The virtual works done by the surface electrical charges of the upper and lower surfaces of the upper and lower piezoelectric patches, δW_Q^u and δW_Q^l , are given by

$$\delta W_Q^u = - \int_S q^u \delta \varphi \, dS = -B_p^u \int_{x_1}^{x_2} q^u \delta V^u \, dx = -Q^u \delta V^u, \quad (15)$$

$$\delta W_Q^l = - \int_S q^l \delta \varphi \, dS = B_p^l \int_{x_1}^{x_2} q^l \delta V^l \, dx = Q^l \delta V^l \quad (16)$$

where q , φ , and S are the electric surface charge, electric potential, and electrode surface, respectively. The patches interfaces with the beam are considered grounded.

The virtual work done by the applied external mechanical load at the tip of the structure is given by

$$\delta W_F = -F_z \delta w_o(L). \quad (17)$$

The virtual work δW of external electrical and mechanical loads is then the sum of those given in Eqs. (15) to (17) so that

$$\delta W = \delta W_Q^u + \delta W_Q^l + \delta W_F. \quad (18)$$

2.3 Segments equations

The above variational Eqs. (14) and (18) are used to derive the balance equations and corresponding electromechanical boundary and continuity conditions that will later be used to describe the DTF approach.

The balance equations are obtained by back-substituting Eqs. (14) and (18), into Eq. (7) and integrating by parts and then collecting terms with common virtual generalized displacements, resulting in three balance equations for each segment.

The balance equations for segment 1 are given by

$$\delta u_o : A_b \tilde{Q}_{11}^b u_o'' = 0, \quad (19)$$

$$\delta \psi : I_b \tilde{Q}_{11}^b \psi'' - k_s A_b \tilde{Q}_{55}^b (\psi + w_o') = 0, \quad (20)$$

$$\delta w_o : k_s A_b \tilde{Q}_{55}^b (\psi' + w_o'') = 0. \quad (21)$$

For segment 2, the balance equations are given by

$$\delta u_o : \left(A_b \tilde{Q}_{11}^b + A_p^u \tilde{Q}_{11}^{pu} + A_p^l \tilde{Q}_{11}^{pl} \right) u_o'' + \left(A_p^u H_2^u \tilde{Q}_{11}^{pu} - A_p^l H_2^l \tilde{Q}_{11}^{pl} \right) \psi'' = 0, \quad (22)$$

$$\delta \psi : \left(A_p^u H_2^u \tilde{Q}_{11}^{pu} - A_p^l H_2^l \tilde{Q}_{11}^{pl} \right) u_o'' + \left(I_b \tilde{Q}_{11}^b + I_p^u \tilde{Q}_{11}^{pu} + I_p^l \tilde{Q}_{11}^{pl} \right) \psi'' - k_s \left(A_b \tilde{Q}_{55}^b + A_p^u \tilde{Q}_{55}^{pu} + A_p^l \tilde{Q}_{55}^{pl} \right) (\psi + w_o') = 0, \quad (23)$$

$$\delta w_o : k_s \left(A_b \tilde{Q}_{55}^b + A_p^u \tilde{Q}_{55}^{pu} + A_p^l \tilde{Q}_{55}^{pl} \right) (\psi' + w_o'') = 0. \quad (24)$$

The following electrical equations hold also for segment 2:

$$\delta V^u : \int_{x_1}^{x_2} \left(A_p^u \tilde{\epsilon}_{33}^u \frac{V^u}{t_p^u} - A_p^u \tilde{e}_{31}^u u_o' - A_p^u H_2^u \tilde{e}_{31}^u \psi' \right) dx = Q^u t_p^u, \quad (25)$$

$$\delta V^l : \int_{x_1}^{x_2} \left(A_p^l \tilde{\epsilon}_{33}^l \frac{V^l}{t_p^l} - A_p^l \tilde{e}_{31}^l u_o' + A_p^l H_2^l \tilde{e}_{31}^l \psi' \right) dx = -Q^l t_p^l. \quad (26)$$

Finally, for segment 3, the balance equations are given by

$$\delta u_o : A_b \tilde{Q}_{11}^b u_o'' = 0, \quad (27)$$

$$\delta \psi : I_b \tilde{Q}_{11}^b \psi'' - k_s A_b \tilde{Q}_{55}^b (\psi + w_o') = 0, \quad (28)$$

$$\delta w_o : k_s A_b \tilde{Q}_{55}^b (\psi' + w_o'') = 0. \quad (29)$$

To simplify the previous balance equations, the following C_i quantities are introduced:

$$C_0 = C_0^b + C_0^{pu} + C_0^{pl}, \quad C_1^p = C_1^{pu} - C_1^{pl}, \quad C_2 = C_2^b + C_2^{pu} + C_2^{pl}, \quad C_3 = C_3^b + C_3^{pu} + C_3^{pl} \quad (30)$$

where C_j^b and C_j^{pk} are defined as

$$\begin{aligned} C_0^{(b,pk)} &= A_{b,p}^k \tilde{Q}_{11}^{(b,pk)}, & C_1^{pk} &= A_p^k H_2^k \tilde{Q}_{11}^{pk}, & C_2^{(b,pk)} &= I_{(b,p)}^k \tilde{Q}_{11}^{(b,pk)}, \\ C_3^{(b,pk)} &= k_s A_{(b,p)}^k \tilde{Q}_{55}^{(b,pk)}, & C_4^{pk} &= B_p^k e_{31}^k, & C_5^{pk} &= B_p^k H_2^k e_{31}^k \end{aligned} \quad (31)$$

with j running from 0 to 5 and k taking the values u and l according to the considered patch.

If considered independent, the mechanical BCs associated with segments 1 and 3, i.e., those associated with Eqs. (19) to (21) and Eqs. (27) to (29), are given by

$$C_0^b u'_o \Big|_0^{x_1} = 0 \quad \text{Or} \quad \delta u_o \Big|_0^{x_1} = 0, \quad (32)$$

$$C_2^b \psi' \Big|_0^{x_1} = 0 \quad \text{Or} \quad \delta \psi \Big|_0^{x_1} = 0, \quad (33)$$

$$\left[C_3^b (\psi + w'_o) \right] \Big|_0^{x_1} = 0 \quad \text{Or} \quad \delta w_o \Big|_0^{x_1} = 0 \quad (34)$$

and

$$C_0^b u'_o \Big|_{x_2}^L = 0 \quad \text{Or} \quad \delta u_o \Big|_{x_2}^L = 0, \quad (35)$$

$$C_2^b \psi' \Big|_{x_2}^L = 0 \quad \text{Or} \quad \delta \psi \Big|_{x_2}^L = 0, \quad (36)$$

$$\left[C_3^b (\psi + w'_o) - F_z \right] \Big|_L - \left[C_3^b (\psi + w'_o) \right] \Big|_{x_2} = 0 \quad \text{Or} \quad \delta w_o \Big|_{x_2}^L = 0 \quad (37)$$

while those of the smart beam part (segment 2), if considered independent, are

$$\left(C_0 u'_o + C_1^p \psi' + C_4^{pu} V^u + C_4^{pl} V^l \right) \Big|_{x_1}^{x_2} = 0 \quad \text{Or} \quad \delta u_o \Big|_{x_1}^{x_2} = 0, \quad (38)$$

$$\left(C_1^p u'_o + C_2 \psi' + C_5^{pu} V^u - C_5^{pl} V^l \right) \Big|_{x_1}^{x_2} = 0 \quad \text{Or} \quad \delta \psi \Big|_{x_1}^{x_2} = 0, \quad (39)$$

$$\left[C_3 (\psi + w'_o) \right] \Big|_{x_1}^{x_2} = 0 \quad \text{Or} \quad \delta w_o \Big|_{x_1}^{x_2} = 0. \quad (40)$$

The CC at sections between segments 1 and 2, at x_1 , and that between segments 2 and 3, at x_2 , (with $i = 1, 2$) are

$$(u_o)_i = (u_o)_{i+1}, \quad (41)$$

$$(\psi)_i = (\psi)_{i+1}, \quad (42)$$

$$(w_o)_i = (w_o)_{i+1}. \quad (43)$$

Besides, the equilibrium conditions at the section connecting segments 1 and 2, i.e., x_1 , are

$$C_0^b u'_o \Big|_{x_1} = \left(C_0 u'_o + C_1^p \psi' + C_4^{pu} V^u + C_4^{pl} V^l \right) \Big|_{x_1}, \quad (44)$$

$$C_2^b \psi' \Big|_{x_1} = \left(C_1^p u'_o + C_2 \psi' + C_5^{pu} V^u - C_5^{pl} V^l \right) \Big|_{x_1}, \quad (45)$$

$$\left[C_3^b (\psi + w'_o) \right] \Big|_{x_1} = \left[C_3 (\psi + w'_o) \right] \Big|_{x_1}, \quad (46)$$

and those at the section connecting segments 2 and 3 are

$$\left(C_0 u'_o + C_1^p \psi' + C_4^{pu} V^u + C_4^{pl} V^l \right) \Big|_{x_2} = C_0^b u'_o \Big|_{x_2}, \quad (47)$$

$$\left(C_1^p u'_o + C_2 \psi' + C_5^{pu} V^u - C_5^{pl} V^l \right) \Big|_{x_2} = C_2^b \psi' \Big|_{x_2}, \quad (48)$$

$$\left[C_3 (\psi + w'_o) \right] \Big|_{x_2} = \left[C_3^b (\psi + w'_o) \right] \Big|_{x_2}. \quad (49)$$

It is worth noting that the C_1^p stiffness parameter couples the membrane-bending adaptive beam responses. It should also be noticed that this coupling parameter is present only in segment 2, which contains the piezoelectric patches, because of the asymmetric (different thickness) configuration of the adaptive beam (see Fig. 1).

The balance equations and associated BC, Eqs. (19) to (40), are now transformed into first-order state space form using the DTF approach in order to derive the two piezoelectric adaptive beam static sensing and actuation problems, which depend on the electric BC.

It can be seen that, for segment 2, the first two balance Eqs. (22) and (23) are coupled and need to be solved for u''_o and ψ'' . Hence, for simplicity, they are first rewritten as

$$\delta u_o : C_0 u''_o + C_1^p \psi'' = 0, \quad (50)$$

$$\delta \psi : C_1^p u''_o + C_2 \psi'' - C_3 (\psi + w'_o) = 0, \quad (51)$$

$$\delta w_o : C_3 (\psi' + w''_o) = 0. \quad (52)$$

The corresponding mechanical BC and CC are those of Eqs. (38) to (40).

From Eq. (50), u''_o can be written as

$$u''_o = -\frac{C_1^p}{C_0} \psi''. \quad (53)$$

Back-substituting this result in Eq. (51) and collecting common terms yields the following expression for ψ'' :

$$\psi'' = C_3 \left(\frac{C_0}{C_2 C_0 - (C_1^p)^2} \psi + \frac{C_0}{C_2 C_0 - (C_1^p)^2} w'_o \right). \quad (54)$$

Now, back-substituting ψ'' from Eq. (54) into Eq. (53) and collecting common terms results in the following expression of u''_o :

$$u''_o = C_3 \left(\frac{-C_1^p}{C_2 C_0 - (C_1^p)^2} \psi + \frac{-C_1^p}{C_2 C_0 - (C_1^p)^2} w'_o \right). \quad (55)$$

As similar expression for w''_o can be obtained by solving Eq. (52), namely

$$w''_o = -\psi' \quad (56)$$

Using the result of ψ'' from Eq. (54), u''_o from Eq. (55) and w''_o from Eq. (56), the balance Eqs. (50)–(52) are rewritten as follows:

$$\begin{aligned} u''_o &= \bar{C}_1^p (\psi + w'_o), \\ \psi'' &= \bar{C}_2 (\psi + w'_o), \\ w''_o &= -\psi' \end{aligned} \quad (57)$$

where \bar{C}_i are given by

$$\bar{C}_1^p = -\frac{C_1^p C_3}{C_2 C_0 - (C_1^p)^2}, \quad \bar{C}_2 = \frac{C_0 C_3}{C_2 C_0 - (C_1^p)^2}. \quad (58)$$

Note that \bar{C}_1^p ensures the membrane-bending coupling, inherited by the presence of C_1^p , that is present only in segment 2, which contains the piezoelectric patches. Hence, it vanishes for segments 1 and 3, for vanishing C_1^p , and the bare beam local Eqs. (19) to (21) and Eqs. (27) to (29) are automatically recovered, as

$$\begin{aligned} u_o'' &= 0, \\ \psi'' &= \bar{C}_2^b (\psi + w_o'), \\ w_o'' &= -\psi' \end{aligned} \quad (59)$$

where \bar{C}_2^b is given by

$$\bar{C}_2^b = \frac{C_3^b}{C_2^b}. \quad (60)$$

3 DTF-based unified static solutions

Applying the appropriate changes to accommodate the new assumptions, the DTF solution [5] is obtained by having the balance equations, and corresponding boundary/equilibrium conditions of the three segments satisfy the following first-order state space equations:

$$\mathbf{Y}_i'(x) = \mathbf{F}_i \mathbf{Y}_i(x), \quad i = 1, 2, 3 \quad (61)$$

where $\mathbf{Y}_i(x) = \{\mathbf{D}(x), \mathbf{D}'_i(x)\}^T$ with $\mathbf{D}(x) = \{u_o, \psi, w_o\}^T$ is the generalized displacements vector and $\mathbf{D}'_i(x) = \{u_o', \psi', w_o'\}^T$ its x -derivative.

Following the same procedure as in [6,7] and from Eqs. (57) and (59), the expressions for \mathbf{F}_i , $i = 1, 2, 3$, modify to

$$\mathbf{F}_2 = \begin{bmatrix} 0 & 0 & 0 & 1 & 0 & 0 \\ 0 & 0 & 0 & 0 & 1 & 0 \\ 0 & 0 & 0 & 0 & 0 & 1 \\ 0 & \bar{C}_1^p & 0 & 0 & 0 & \bar{C}_1^p \\ 0 & \bar{C}_2^b & 0 & 0 & 0 & \bar{C}_2^b \\ 0 & 0 & 0 & 0 & -1 & 0 \end{bmatrix}, \quad \mathbf{F}_{1,3} = \begin{bmatrix} 0 & 0 & 0 & 1 & 0 & 0 \\ 0 & 0 & 0 & 0 & 1 & 0 \\ 0 & 0 & 0 & 0 & 0 & 1 \\ 0 & 0 & 0 & 0 & 0 & 0 \\ 0 & \bar{C}_2^b & 0 & 0 & 0 & \bar{C}_2^b \\ 0 & 0 & 0 & 0 & -1 & 0 \end{bmatrix}. \quad (62)$$

The solution of Eq. (61) is obtained by having $\mathbf{Y}_i(x)$ expressed as

$$\mathbf{Y}_i(x) = \mathbf{H}_i(x) \boldsymbol{\gamma}_i \quad (63)$$

with $\mathbf{H}_i(x)$ being a 6×6 matrix given by

$$\mathbf{H}_i(x) = e^{\mathbf{F}_i x} \left[\mathbf{M}_i e^{\mathbf{F}_i x_{i-1}} + \mathbf{N}_i e^{\mathbf{F}_i x_i} \right]^{-1} \quad i = 1, 2, 3, \quad (64)$$

and $\mathbf{M}_i, \mathbf{N}_i$ are linked to $\boldsymbol{\gamma}_i$ by the following matrix boundary/continuity equation:

$$\boldsymbol{\gamma}_i = \mathbf{M}_i \mathbf{Y}_i(x_{i-1}) + \mathbf{N}_i \mathbf{Y}_i(x_i), \quad (65)$$

Hence, for $i = 1$, Eq. (65) reduces to

$$\boldsymbol{\gamma}_1 = \mathbf{M}_1 \mathbf{Y}_1(x_0) + \mathbf{N}_1 \mathbf{Y}_1(x_1) \quad (66)$$

which represents the boundary/continuity conditions at the edges of segment 1, x_0 and x_1 .

Since the beam is clamped at $x_0 = 0$, the product $\mathbf{M}_1 \mathbf{Y}_1(0)$ must have the following form:

$$\mathbf{M}_1 \mathbf{Y}_1(0) = \begin{bmatrix} 1 & 0 & 0 & 0 & 0 & 0 \\ 0 & 1 & 0 & 0 & 0 & 0 \\ 0 & 0 & 1 & 0 & 0 & 0 \\ 0 & 0 & 0 & 0 & 0 & 0 \\ 0 & 0 & 0 & 0 & 0 & 0 \\ 0 & 0 & 0 & 0 & 0 & 0 \end{bmatrix} \begin{Bmatrix} u_o(0) \\ \psi(0) \\ w_o(0) \\ u_o'(0) \\ \psi'(0) \\ w_o'(0) \end{Bmatrix} = \begin{bmatrix} \mathbf{I} & \mathbf{0} \\ \mathbf{0} & \mathbf{0} \end{bmatrix} \left\{ \begin{Bmatrix} \mathbf{D}(x_0) \\ \mathbf{D}'_1(x_0) \end{Bmatrix} \right\}. \quad (67)$$

From the displacements continuity at x_1 , Eqs. (41)–(43), the following $\mathbf{N}_1 \mathbf{Y}_1(x_1)$ must be satisfied:

$$\mathbf{N}_1 \mathbf{Y}_1(x_1) = \begin{bmatrix} 0 & 0 & 0_1' & 0 & 0 & 0 \\ 0 & 0 & 0_1 & 0 & 0 & 0 \\ 0 & 0 & 0_1' & 0 & 0 & 0 \\ 1^- & 0^- & 0_1^+ & 0^- & 0^- & 0^- \\ 0 & 1 & 0_1 & 0 & 0 & 0 \\ 0 & 0 & 1_1' & 0 & 0 & 0 \end{bmatrix} \begin{Bmatrix} u_o(x_1) \\ \psi(x_1) \\ w_o(x_1) \\ u_o'(x_1) \\ \psi'(x_1) \\ w_o'(x_1) \end{Bmatrix} = \begin{bmatrix} \mathbf{0}'\mathbf{0} \\ \mathbf{I}'\mathbf{0} \end{bmatrix} \left\{ \begin{array}{l} \mathbf{D}(x_1) \\ \mathbf{D}'_1(x_1) \end{array} \right\} \quad (68)$$

where \mathbf{I} is a 3×3 identity matrix.

The resulting expression of $\boldsymbol{\gamma}_1$ is therefore

$$\boldsymbol{\gamma}_1 = \begin{bmatrix} \mathbf{I}'\mathbf{0} \\ \mathbf{0}'\mathbf{0} \end{bmatrix} \left\{ \begin{array}{l} \mathbf{D}(x_0) \\ \mathbf{D}'_1(x_0) \end{array} \right\} + \begin{bmatrix} \mathbf{0}'\mathbf{0} \\ \mathbf{I}'\mathbf{0} \end{bmatrix} \left\{ \begin{array}{l} \mathbf{D}(x_1) \\ \mathbf{D}'_1(x_1) \end{array} \right\}, \quad (69)$$

which, when expanded, results in

$$\boldsymbol{\gamma}_1 = \left\{ \begin{array}{l} \mathbf{D}(x_0) \\ \mathbf{D}'(x_1) \end{array} \right\}. \quad (70)$$

Note that the upper part of Eq. (70) satisfies the BC at $x = 0$, the right hand side of Eqs. (32) to (34), and hence the expression $\mathbf{D}(x_0)$ is identically equal to zero. Therefore, $\boldsymbol{\gamma}_1$ reduces to

$$\boldsymbol{\gamma}_1 = \left\{ \begin{array}{l} \mathbf{0} \\ \mathbf{D}'(x_1) \end{array} \right\}. \quad (71)$$

It should be noted that $\boldsymbol{\gamma}_1$ vector represents the displacement BC and CC at the edges of segment 1 with the upper vector representing the generalized displacement BC at x_0 and the lower vector representing the generalized displacement CC at x_1 .

Similarly, for $i = 2$, Eq. (65) reduces to

$$\boldsymbol{\gamma}_2 = \mathbf{M}_2 \mathbf{Y}_2(x_1) + \mathbf{N}_2 \mathbf{Y}_2(x_2). \quad (72)$$

Since the displacements are continuous at both edges of segment 2, namely at x_1 and x_2 , the following expression of $\boldsymbol{\gamma}_2$ vector must be satisfied:

$$\boldsymbol{\gamma}_2 = \begin{bmatrix} \mathbf{I}'\mathbf{0} \\ \mathbf{0}'\mathbf{0} \end{bmatrix} \left\{ \begin{array}{l} \mathbf{D}(x_1) \\ \mathbf{D}'_2(x_1) \end{array} \right\} + \begin{bmatrix} \mathbf{0}'\mathbf{0} \\ \mathbf{I}'\mathbf{0} \end{bmatrix} \left\{ \begin{array}{l} \mathbf{D}(x_2) \\ \mathbf{D}'_2(x_2) \end{array} \right\} \quad (73)$$

which when expanded reduces to

$$\boldsymbol{\gamma}_2 = \left\{ \begin{array}{l} \mathbf{D}(x_1) \\ \mathbf{D}'(x_2) \end{array} \right\}. \quad (74)$$

Here, the upper vector of Eq. (74) represents the generalized displacement CC at x_1 and the lower vector represents the generalized displacement CC at x_2 .

Finally, for $i = 3$, Eq. (65) reduces to

$$\boldsymbol{\gamma}_3 = \mathbf{M}_3 \mathbf{Y}_3(x_2) + \mathbf{N}_3 \mathbf{Y}_3(x_3 = L) \quad (75)$$

where the expression for $\boldsymbol{\gamma}_3$ is obtained by satisfying the generalized displacements continuity at x_2 and the vertical force end conditions at $x_3 = L$, Eqs. (41) to (43), and left of Eqs. (35) to (37).

Thus, from the generalized displacements CC, the product $\mathbf{M}_3 \mathbf{Y}_3(x_2)$ must have the following form:

$$\mathbf{M}_3 \mathbf{Y}_3(x_2) = \begin{bmatrix} 1 & 0 & 0_1' & 0 & 0 & 0 \\ 0 & 1 & 0_1 & 0 & 0 & 0 \\ 0 & 0 & 1_1' & 0 & 0 & 0 \\ 0^- & 0^- & 0_1^+ & 0^- & 0^- & 0^- \\ 0 & 0 & 0_1 & 0 & 0 & 0 \\ 0 & 0 & 0_1' & 0 & 0 & 0 \end{bmatrix} \begin{Bmatrix} u_o(x_2) \\ \psi(x_2) \\ w_o(x_2) \\ u_o'(x_2) \\ \psi'(x_2) \\ w_o'(x_2) \end{Bmatrix} = \begin{bmatrix} \mathbf{I}'\mathbf{0} \\ \mathbf{0}'\mathbf{0} \end{bmatrix} \left\{ \begin{array}{l} \mathbf{D}(x_2) \\ \mathbf{D}'_3(x_2) \end{array} \right\}. \quad (76)$$

Since the generalized displacements at $x_3 = L$ are unknown, the left hand side of Eqs. (35) to (37) must be equal to the natural BC; thus, the product $\mathbf{N}_3 \mathbf{Y}_3(x_3 = L)$ changes to

$$\mathbf{N}_3 \mathbf{Y}_3(L) = \begin{bmatrix} 0 & 0 & 0 & 0 & 0 & 0 \\ 0 & 0 & 0 & 0 & 0 & 0 \\ 0 & 0 & 0 & 0 & 0 & 0 \\ 0 & 0 & 0 & C_0^b & 0 & 0 \\ 0 & 0 & 0 & 0 & C_2^b & 0 \\ 0 & C_3^b & 0 & 0 & 0 & C_3^b \end{bmatrix} \begin{Bmatrix} u_o(L) \\ \psi(L) \\ w_o(L) \\ u_o^r(L) \\ \psi^r(L) \\ w_o^r(L) \end{Bmatrix} = \begin{bmatrix} \mathbf{0} & \mathbf{0} \\ \mathbf{B}_D^3 & \mathbf{B}_{D'}^3 \end{bmatrix} \begin{Bmatrix} \mathbf{D}(L) \\ \mathbf{D}'_3(L) \end{Bmatrix}. \quad (77)$$

Using the results from Eqs. (76) and (77), $\boldsymbol{\gamma}_3$ reduces to

$$\boldsymbol{\gamma}_3 = \begin{bmatrix} \mathbf{I} & \mathbf{0} \\ \mathbf{0} & \mathbf{0} \end{bmatrix} \begin{Bmatrix} \mathbf{D}(x_2) \\ \mathbf{D}'_3(x_2) \end{Bmatrix} + \begin{bmatrix} \mathbf{0} & \mathbf{0} \\ \mathbf{B}_D^3 & \mathbf{B}_{D'}^3 \end{bmatrix} \begin{Bmatrix} \mathbf{D}(L) \\ \mathbf{D}'_3(L) \end{Bmatrix} \quad (78)$$

which simplifies to

$$\boldsymbol{\gamma}_3 = \begin{Bmatrix} \mathbf{D}(x_2) \\ \mathbf{B}_D^3 \mathbf{D}(L) + \mathbf{B}_{D'}^3 \mathbf{D}'_3(L) \end{Bmatrix}. \quad (79)$$

Note that the lower part of Eq. (79) should satisfy the natural BC at $x_3 = L$, Eq. (35) to (37); hence, the expression $\mathbf{B}_D^3 \mathbf{D}(L) + \mathbf{B}_{D'}^3 \mathbf{D}'_3(L)$ is identically equal to \mathbf{F} , with $\mathbf{F} = \{0, 0, F_z\}^T$.

Therefore, $\boldsymbol{\gamma}_3$ reduces to

$$\boldsymbol{\gamma}_3 = \begin{Bmatrix} \mathbf{D}(x_2) \\ \mathbf{F} \end{Bmatrix}. \quad (80)$$

From Eqs. (44) to (49), the equilibrium conditions at the boundaries of segments 1, 2, and 3 can generally be expressed (after considering the CC (41)-(43)) as

$$\mathbf{B}_D^i \mathbf{D}(x_i) + \mathbf{B}_{D'}^i \mathbf{D}'_i(x_i) + \tilde{\mathbf{V}}_i = \mathbf{B}_D^{i+1} \mathbf{D}(x_i) + \mathbf{B}_{D'}^{i+1} \mathbf{D}'_{i+1}(x_i) + \tilde{\mathbf{V}}_{i+1} \quad i = 1, 2. \quad (81)$$

Note that $\tilde{\mathbf{V}}$ exists only for segment 2, and from Eqs. (44) to (46), it is given by

$$\tilde{\mathbf{V}} = \begin{Bmatrix} C_4^{pu} \\ C_5^{bu} \end{Bmatrix} V^u + \begin{Bmatrix} C_4^{pl} \\ -C_5^{pl} \\ 0 \end{Bmatrix} V^l. \quad (82)$$

For $i = 1$, the equilibrium conditions at x_1 between segments 1 and 2 expand to

$$\mathbf{B}_D^1 \mathbf{D}(x_1) + \mathbf{B}_{D'}^1 \mathbf{D}'_1(x_1) = \mathbf{B}_D^2 \mathbf{D}(x_1) + \mathbf{B}_{D'}^2 \mathbf{D}'_2(x_1) + \tilde{\mathbf{V}} \quad (83)$$

with \mathbf{B}_D^1 , $\mathbf{B}_{D'}^1$, \mathbf{B}_D^2 , and $\mathbf{B}_{D'}^2$ obtained from Eqs. (44) to (46) as

$$\mathbf{B}_D^1 = \begin{bmatrix} 0 & 0 & 0 \\ 0 & 0 & 0 \\ 0 & C_3^b & 0 \end{bmatrix}, \quad \mathbf{B}_{D'}^1 = \begin{bmatrix} C_0^b & 0 & 0 \\ 0 & C_2^b & 0 \\ 0 & 0 & C_3^b \end{bmatrix}, \quad \mathbf{B}_D^2 = \begin{bmatrix} 0 & 0 & 0 \\ 0 & 0 & 0 \\ 0 & C_3 & 0 \end{bmatrix}, \quad \mathbf{B}_{D'}^2 = \begin{bmatrix} C_0 & C_1^p & 0 \\ C_1^p & C_2 & 0 \\ 0 & 0 & C_3 \end{bmatrix}. \quad (84)$$

Similarly, the equilibrium conditions at x_2 between segments 2 and 3, i.e., $i = 2$, expand to

$$\mathbf{B}_D^2 \mathbf{D}(x_2) + \mathbf{B}_{D'}^2 \mathbf{D}'_2(x_2) + \tilde{\mathbf{V}} = \mathbf{B}_D^3 \mathbf{D}(x_2) + \mathbf{B}_{D'}^3 \mathbf{D}'_3(x_2) \quad (85)$$

with \mathbf{B}_D^3 , and $\mathbf{B}_{D'}^3$ obtained from Eq. (77); it can be noticed that they are equal to those of segment 1 which is normal since both segments represent the bare beam parts.

The vectors $\mathbf{D}'_1(x_1)$, $\mathbf{D}'_2(x_1)$, $\mathbf{D}'_2(x_2)$, and $\mathbf{D}'_3(x_2)$ of Eqs. (83) and (85) can be written in terms of vectors $\mathbf{D}(x_1)$ and $\mathbf{D}(x_2)$ by expanding Eq. (63) in the following form:

$$\begin{Bmatrix} \mathbf{D}(x) \\ \mathbf{D}'_i(x) \end{Bmatrix} = \begin{bmatrix} \mathbf{H}_{aa}^i(x) & \mathbf{H}_{ab}^i(x) \\ \mathbf{H}_{ba}^i(x) & \mathbf{H}_{bb}^i(x) \end{bmatrix} \{\boldsymbol{\gamma}_i\}. \quad (86)$$

Thus, for segment 1 Eq. (86), written at the segment's right end, is (after Eq. (71))

$$\begin{Bmatrix} \mathbf{D}(x_1) \\ \mathbf{D}'_1(x_1) \end{Bmatrix} = \begin{bmatrix} \mathbf{H}_{qa}^1(x_1) & \mathbf{H}_{qb}^1(x_1) \\ \mathbf{H}_{ba}^1(x_1) & \mathbf{H}_{bb}^1(x_1) \end{bmatrix} \begin{Bmatrix} \mathbf{0} \\ \mathbf{D}(x_1) \end{Bmatrix} \quad (87)$$

from which $\mathbf{D}'_1(x_1)$ is found to be

$$\mathbf{D}'_1(x_1) = \mathbf{H}_{bb}^1(x_1) \mathbf{D}(x_1). \quad (88)$$

Similarly, for segment 2 and using Eqs. (74), (86) written at this segment's ends, x_1 and x_2 , provides, respectively

$$\begin{Bmatrix} \mathbf{D}(x_1) \\ \mathbf{D}'_2(x_1) \end{Bmatrix} = \begin{bmatrix} \mathbf{H}_{qa}^2(x_1) & \mathbf{H}_{qb}^2(x_1) \\ \mathbf{H}_{ba}^2(x_1) & \mathbf{H}_{bb}^2(x_1) \end{bmatrix} \begin{Bmatrix} \mathbf{D}(x_1) \\ \mathbf{D}(x_2) \end{Bmatrix}, \quad (89)$$

$$\begin{Bmatrix} \mathbf{D}(x_2) \\ \mathbf{D}'_2(x_2) \end{Bmatrix} = \begin{bmatrix} \mathbf{H}_{qa}^2(x_2) & \mathbf{H}_{qb}^2(x_2) \\ \mathbf{H}_{ba}^2(x_2) & \mathbf{H}_{bb}^2(x_2) \end{bmatrix} \begin{Bmatrix} \mathbf{D}(x_1) \\ \mathbf{D}(x_2) \end{Bmatrix} \quad (90)$$

from which $\mathbf{D}'_2(x_1)$ and $\mathbf{D}'_2(x_2)$ are deduced, respectively, as

$$\mathbf{D}'_2(x_1) = \mathbf{H}_{ba}^2(x_1) \mathbf{D}(x_1) + \mathbf{H}_{bb}^2(x_1) \mathbf{D}(x_2), \quad (91)$$

$$\mathbf{D}'_2(x_2) = \mathbf{H}_{ba}^2(x_2) \mathbf{D}(x_1) + \mathbf{H}_{bb}^2(x_2) \mathbf{D}(x_2). \quad (92)$$

Finally, for segment 3, Eq. (86), written at the segment's left end, is now (using Eq. (80))

$$\begin{Bmatrix} \mathbf{D}(x_2) \\ \mathbf{D}'_3(x_2) \end{Bmatrix} = \begin{bmatrix} \mathbf{H}_{aa}^3(x_2) & \mathbf{H}_{ab}^3(x_2) \\ \mathbf{H}_{ba}^3(x_2) & \mathbf{H}_{bb}^3(x_2) \end{bmatrix} \begin{Bmatrix} \mathbf{D}(x_2) \\ \mathbf{F} \end{Bmatrix} \quad (93)$$

from which $\mathbf{D}'_3(x_2)$ is

$$\mathbf{D}'_3(x_2) = \mathbf{H}_{ba}^3(x_2) \mathbf{D}(x_2) + \mathbf{H}_{bb}^3(x_2) \mathbf{F}. \quad (94)$$

Substituting Eqs. (88), (91),(92), and (94) back into Eqs. (83) and (85) and collecting terms yields

$$\begin{bmatrix} \mathbf{K}_{11}^{SC} & \mathbf{K}_{12}^{SC} \\ \mathbf{K}_{21}^{SC} & \mathbf{K}_{22}^{SC} \end{bmatrix} \begin{Bmatrix} \mathbf{D}(x_1) \\ \mathbf{D}(x_2) \end{Bmatrix} = \begin{Bmatrix} \mathbf{0} \\ \mathbf{B}_{D'}^3, \mathbf{H}_{bb}^3(x_2) \mathbf{F} \end{Bmatrix} + \begin{Bmatrix} \tilde{\mathbf{V}} \\ -\tilde{\mathbf{V}} \end{Bmatrix} \quad (95)$$

where the SC, for $\tilde{\mathbf{V}} = 0$, stiffness matrix is given by

$$\begin{bmatrix} \mathbf{K}_{11}^{SC} & \mathbf{K}_{12}^{SC} \\ \mathbf{K}_{21}^{SC} & \mathbf{K}_{22}^{SC} \end{bmatrix} = \begin{bmatrix} \mathbf{B}_D^1 + \mathbf{B}_{D'}^1 \mathbf{H}_{bb}^1(x_1) - \mathbf{B}_D^2 - \mathbf{B}_{D'}^2 \mathbf{H}_{ba}^2(x_1) & -\mathbf{B}_{D'}^2 \mathbf{H}_{bb}^2(x_1) \\ \mathbf{B}_{D'}^2 \mathbf{H}_{ba}^2(x_2) & \mathbf{B}_D^2 + \mathbf{B}_{D'}^2 \mathbf{H}_{bb}^2(x_2) - \mathbf{B}_D^3 - \mathbf{B}_{D'}^3 \mathbf{H}_{ba}^3(x_2) \end{bmatrix}. \quad (96)$$

Carrying out the integration at the left hand sides of Eqs. (25) and (26), using Definitions (31) and solving for V^u and V^l , yields

$$V^u = \frac{t_p^u}{B_p^u \tilde{\epsilon}_{33}^{Su} L_p} \left\{ [C_4^{pu} u_o(x_2) + C_5^{pu} \psi(x_2)] - [C_4^{pu} u_o(x_1) + C_5^{pu} \psi(x_1)] + Q^u \right\}, \quad (97)$$

and

$$V^l = \frac{t_p^l}{B_p^l \tilde{\epsilon}_{33}^{Sl} L_p} \left\{ [C_4^{pl} u_o(x_2) - C_5^{pl} \psi(x_2)] - [C_4^{pl} u_o(x_1) - C_5^{pl} \psi(x_1)] - Q^l \right\}. \quad (98)$$

Equations (97) and (98) can be rewritten as

$$V^u = \frac{t_p^u}{B_p^u \tilde{\epsilon}_{33}^{Su} L_p} \left([C_4^{pu} \ C_5^{pu} \ 0] \begin{Bmatrix} u_o(x_2) \\ \psi(x_2) \\ w_o(x_2) \end{Bmatrix} - [C_4^{pu} \ C_5^{pu} \ 0] \begin{Bmatrix} u_o(x_1) \\ \psi(x_1) \\ w_o(x_1) \end{Bmatrix} + Q^u \right) \quad (99)$$

and

$$V^l = \frac{t_p^l}{B_p^l \tilde{\epsilon}_{33}^l L_p} \left([C_4^{pl} - C_5^{pl} \ 0] \begin{Bmatrix} u_o(x_2) \\ \psi(x_2) \\ w_o(x_2) \end{Bmatrix} - [C_4^{pl} - C_5^{pl} \ 0] \begin{Bmatrix} u_o(x_1) \\ \psi(x_1) \\ w_o(x_1) \end{Bmatrix} - Q^l \right). \quad (100)$$

Back-substituting the voltages (99) and (100) into $\tilde{\mathbf{V}}$, Eq. (82), yields

$$\begin{aligned} \tilde{\mathbf{V}} = & C_6^u \left(\begin{bmatrix} (C_4^{pu})^2 & C_4^{pu} C_5^{pu} & 0 \\ C_4^{pu} C_5^{pu} & (C_5^{pu})^2 & 0 \\ 0 & 0 & 0 \end{bmatrix} \begin{Bmatrix} u_o(x_2) \\ \psi(x_2) \\ w_o(x_2) \end{Bmatrix} - \begin{bmatrix} (C_4^{pu})^2 & C_4^{pu} C_5^{pu} & 0 \\ C_4^{pu} C_5^{pu} & (C_5^{pu})^2 & 0 \\ 0 & 0 & 0 \end{bmatrix} \begin{Bmatrix} u_o(x_1) \\ \psi(x_1) \\ w_o(x_1) \end{Bmatrix} \right) \\ & + C_6^l \left(\begin{bmatrix} (C_4^{pl})^2 & -C_4^{pl} C_5^{pl} & 0 \\ -C_4^{pl} C_5^{pl} & (C_5^{pl})^2 & 0 \\ 0 & 0 & 0 \end{bmatrix} \begin{Bmatrix} u_o(x_2) \\ \psi(x_2) \\ w_o(x_2) \end{Bmatrix} - \begin{bmatrix} (C_4^{pl})^2 & -C_4^{pl} C_5^{pl} & 0 \\ -C_4^{pl} C_5^{pl} & (C_5^{pl})^2 & 0 \\ 0 & 0 & 0 \end{bmatrix} \begin{Bmatrix} u_o(x_1) \\ \psi(x_1) \\ w_o(x_1) \end{Bmatrix} \right) \\ & + C_6^u \begin{Bmatrix} C_4^{pu} \\ C_5^{pu} \\ 0 \end{Bmatrix} Q^u - C_6^l \begin{Bmatrix} C_4^{pl} \\ -C_5^{pl} \\ 0 \end{Bmatrix} Q^l \end{aligned} \quad (101)$$

with C_6^u and C_6^l defined as

$$C_6^u = \frac{t_p^u}{B_p^u \tilde{\epsilon}_{33}^u L_p}, \quad C_6^l = \frac{t_p^l}{B_p^l \tilde{\epsilon}_{33}^l L_p}. \quad (102)$$

Equation (101) can be simplified to

$$\tilde{\mathbf{V}} = [\mathbf{B}_{oc}] \{\mathbf{D}(x_2)\} - [\mathbf{B}_{oc}] \{\mathbf{D}(x_1)\} + \tilde{\mathbf{Q}} \quad (103)$$

with \mathbf{B}_{oc} given by

$$\mathbf{B}_{oc} = C_6^u \begin{bmatrix} (C_4^{pu})^2 & C_4^{pu} C_5^{pu} & 0 \\ C_4^{pu} C_5^{pu} & (C_5^{pu})^2 & 0 \\ 0 & 0 & 0 \end{bmatrix} + C_6^l \begin{bmatrix} (C_4^{pl})^2 & -C_4^{pl} C_5^{pl} & 0 \\ -C_4^{pl} C_5^{pl} & (C_5^{pl})^2 & 0 \\ 0 & 0 & 0 \end{bmatrix} \quad (104)$$

and $\tilde{\mathbf{Q}}$ given by

$$\tilde{\mathbf{Q}} = C_6^u \begin{Bmatrix} C_4^{pu} \\ C_5^{pu} \\ 0 \end{Bmatrix} Q^u - C_6^l \begin{Bmatrix} C_4^{pl} \\ -C_5^{pl} \\ 0 \end{Bmatrix} Q^l. \quad (105)$$

Using Eq. (103), the electric contribution of the right hand side of Eq. (95) can be written as

$$\begin{Bmatrix} \tilde{\mathbf{V}} \\ -\tilde{\mathbf{V}} \end{Bmatrix} = - \begin{bmatrix} \mathbf{B}_{oc} & -\mathbf{B}_{oc} \\ -\mathbf{B}_{oc} & \mathbf{B}_{oc} \end{bmatrix} \begin{Bmatrix} \mathbf{D}(x_1) \\ \mathbf{D}(x_2) \end{Bmatrix} + \begin{Bmatrix} \tilde{\mathbf{Q}} \\ -\tilde{\mathbf{Q}} \end{Bmatrix}. \quad (106)$$

Back-substituting Eq. (106) into Eq. (95) and collecting terms yields

$$\begin{bmatrix} \mathbf{K}_{11}^{OC} & \mathbf{K}_{12}^{OC} \\ \mathbf{K}_{21}^{OC} & \mathbf{K}_{22}^{OC} \end{bmatrix} \begin{Bmatrix} \mathbf{D}(x_1) \\ \mathbf{D}(x_2) \end{Bmatrix} = \begin{Bmatrix} \mathbf{0} \\ \mathbf{B}_{D'}^3 \mathbf{H}_{bb}^3(x_2) \mathbf{F} \end{Bmatrix} + \begin{Bmatrix} \tilde{\mathbf{Q}} \\ -\tilde{\mathbf{Q}} \end{Bmatrix} \quad (107)$$

where, the OC for $\tilde{\mathbf{Q}} = \mathbf{0}$, stiffness matrix is given by

$$\begin{bmatrix} \mathbf{K}_{11}^{OC} & \mathbf{K}_{12}^{OC} \\ \mathbf{K}_{21}^{OC} & \mathbf{K}_{22}^{OC} \end{bmatrix} = \begin{bmatrix} \mathbf{K}_{11}^{SC} & \mathbf{K}_{12}^{SC} \\ \mathbf{K}_{21}^{SC} & \mathbf{K}_{22}^{SC} \end{bmatrix} + \begin{bmatrix} \mathbf{B}_{oc} & -\mathbf{B}_{oc} \\ -\mathbf{B}_{oc} & \mathbf{B}_{oc} \end{bmatrix}. \quad (108)$$

3.1 Short-/open-circuit sensing

For both SC and OC static sensing problems, the applied tip force vector \mathbf{F} has to be nonzero; thus, for SC case ($\tilde{\mathbf{V}} = \mathbf{0}$), Eq. (95) reduces to

$$\begin{bmatrix} \mathbf{K}_{11}^{SC} & \mathbf{K}_{12}^{SC} \\ \mathbf{K}_{21}^{SC} & \mathbf{K}_{22}^{SC} \end{bmatrix} \begin{Bmatrix} \mathbf{D}(x_1) \\ \mathbf{D}(x_2) \end{Bmatrix} = \begin{Bmatrix} \mathbf{0} \\ \mathbf{B}_{D'}^3 \mathbf{H}_{bb}^3(x_2) \mathbf{F} \end{Bmatrix}. \quad (109)$$

As a result, the induced charges can be calculated using Eq. (106) by setting ($\tilde{\mathbf{V}} = \mathbf{0}$), namely

$$\begin{Bmatrix} \tilde{\mathbf{Q}} \\ -\tilde{\mathbf{Q}} \end{Bmatrix} = \begin{bmatrix} \mathbf{B}_{oc} & -\mathbf{B}_{oc} \\ -\mathbf{B}_{oc} & \mathbf{B}_{oc} \end{bmatrix} \begin{Bmatrix} \mathbf{D}(x_1) \\ \mathbf{D}(x_2) \end{Bmatrix} \quad (110)$$

with the displacements $\mathbf{D}(x_1)$ and $\mathbf{D}(x_2)$ obtained from Eq. (109), namely

$$\begin{Bmatrix} \mathbf{D}(x_1) \\ \mathbf{D}(x_2) \end{Bmatrix} = \begin{bmatrix} \mathbf{K}_{11}^{SC} & \mathbf{K}_{12}^{SC} \\ \mathbf{K}_{21}^{SC} & \mathbf{K}_{22}^{SC} \end{bmatrix}^{-1} \begin{Bmatrix} \mathbf{0} \\ \mathbf{B}_{D'}^3 \mathbf{H}_{bb}^3(x_2) \mathbf{F} \end{Bmatrix}. \quad (111)$$

The developed SC sensing electric charges on the patches electrodes are obtained by back-substituting Eq. (111) into Eq. (110), namely

$$\begin{Bmatrix} \tilde{\mathbf{Q}} \\ -\tilde{\mathbf{Q}} \end{Bmatrix} = \begin{bmatrix} \mathbf{B}_{oc} & -\mathbf{B}_{oc} \\ -\mathbf{B}_{oc} & \mathbf{B}_{oc} \end{bmatrix} \begin{bmatrix} \mathbf{K}_{11}^{SC} & \mathbf{K}_{12}^{SC} \\ \mathbf{K}_{21}^{SC} & \mathbf{K}_{22}^{SC} \end{bmatrix}^{-1} \begin{Bmatrix} \mathbf{0} \\ \mathbf{B}_{D'}^3 \mathbf{H}_{bb}^3(x_2) \mathbf{F} \end{Bmatrix}, \quad (112)$$

To determine the induced charge on the surface of any of the piezoelectric patches, an additional step is required. This can be done by using Eq. (105) and assuming that the developed charges on the surfaces of both piezoelectric patches are equal and opposite, namely $Q^u = Q$ and $Q^l = -Q$. As a result, the charge vector of Eq. (105) reduces to

$$\tilde{\mathbf{Q}} = \begin{Bmatrix} C_6^u C_4^{pu} - C_6^l C_4^{pl} \\ C_6^u C_5^{pu} + C_6^l C_5^{pl} \\ 0 \end{Bmatrix} Q, \quad (113)$$

and the corresponding induced charge on the surfaces of any of the patches is

$$Q = \frac{\tilde{\mathbf{Q}}(1)}{C_6^u C_4^{pu} - C_6^l C_4^{pl}}, \quad \text{or} \quad Q = \frac{\tilde{\mathbf{Q}}(2)}{C_6^u C_5^{pu} + C_6^l C_5^{pl}}, \quad (114)$$

where $\tilde{\mathbf{Q}}(1)$ and $\tilde{\mathbf{Q}}(2)$ are the first and second elements of the sensed electric charges $\tilde{\mathbf{Q}}$ of Eq. (112).

In the case of OC static sensing ($\tilde{\mathbf{Q}} = \mathbf{0}$), Eq. (107) reduces to

$$\begin{bmatrix} \mathbf{K}_{11}^{OC} & \mathbf{K}_{12}^{OC} \\ \mathbf{K}_{21}^{OC} & \mathbf{K}_{22}^{OC} \end{bmatrix} \begin{Bmatrix} \mathbf{D}(x_1) \\ \mathbf{D}(x_2) \end{Bmatrix} = \begin{Bmatrix} \mathbf{0} \\ \mathbf{B}_{D'}^3 \mathbf{H}_{bb}^3(x_2) \mathbf{F} \end{Bmatrix}. \quad (115)$$

The sensed electric voltages in this case are given by (see Eq. (106) with $\tilde{\mathbf{Q}} = \mathbf{0}$)

$$\begin{Bmatrix} \tilde{\mathbf{V}} \\ -\tilde{\mathbf{V}} \end{Bmatrix} = - \begin{bmatrix} \mathbf{B}_{oc} & -\mathbf{B}_{oc} \\ -\mathbf{B}_{oc} & \mathbf{B}_{oc} \end{bmatrix} \begin{Bmatrix} \mathbf{D}(x_1) \\ \mathbf{D}(x_2) \end{Bmatrix} \quad (116)$$

where the corresponding displacements $\mathbf{D}(x_1)$ and $\mathbf{D}(x_2)$ are obtained by solving Eq. (115), namely

$$\begin{Bmatrix} \mathbf{D}(x_1) \\ \mathbf{D}(x_2) \end{Bmatrix} = \begin{bmatrix} \mathbf{K}_{11}^{OC} & \mathbf{K}_{12}^{OC} \\ \mathbf{K}_{21}^{OC} & \mathbf{K}_{22}^{OC} \end{bmatrix}^{-1} \begin{Bmatrix} \mathbf{0} \\ \mathbf{B}_{D'}^3 \mathbf{H}_{bb}^3(x_2) \mathbf{F} \end{Bmatrix}. \quad (117)$$

Back-substituting these displacements into Eq. (116) results in the following expression for the electric voltages vectors:

$$\begin{Bmatrix} \tilde{\mathbf{V}} \\ -\tilde{\mathbf{V}} \end{Bmatrix} = - \begin{bmatrix} \mathbf{B}_{oc} & -\mathbf{B}_{oc} \\ -\mathbf{B}_{oc} & \mathbf{B}_{oc} \end{bmatrix} \begin{bmatrix} \mathbf{K}_{11}^{OC} & \mathbf{K}_{12}^{OC} \\ \mathbf{K}_{21}^{OC} & \mathbf{K}_{22}^{OC} \end{bmatrix}^{-1} \begin{Bmatrix} \mathbf{0} \\ \mathbf{B}_{D'}^3 \mathbf{H}_{bb}^3(x_2) \mathbf{F} \end{Bmatrix}. \quad (118)$$

To determine the induced voltages by any of the piezoelectric patches, an additional step is required. This can be done by using Eq. (82) and assuming that the induced voltages across both patches are equal and opposite, namely $V^u = V$ and $V^l = -V$. As a result, the voltage vector of Eq. (82) reduces to

$$\tilde{\mathbf{V}} = \begin{Bmatrix} C_4^{pu} - C_4^{pl} \\ C_5^{pu} + C_5^{pl} \\ 0 \end{Bmatrix} V, \quad (119)$$

and the corresponding induced voltage across any of the patches is

$$V = \frac{\tilde{\mathbf{V}}(1)}{C_4^{pu} - C_4^{pl}}, \quad \text{or} \quad V = \frac{\tilde{\mathbf{V}}(2)}{C_5^{pu} + C_5^{pl}} \quad (120)$$

where $\tilde{\mathbf{V}}(1)$ and $\tilde{\mathbf{V}}(2)$ are the first and second elements of the voltage vector $\tilde{\mathbf{V}}$ of Eq. (118).

For both SC and OC sensing problems, the generalized displacements at the tip of the beam ($x_3 = L$) can be obtained using Eq. (63) for $i = 3$, namely

$$\mathbf{Y}_3(x_3) = \mathbf{H}_3(x_3) \boldsymbol{\gamma}_3 \quad (121)$$

where $\mathbf{H}_3(x_3)$ is given by Eq. (64) and $\boldsymbol{\gamma}_3$ is given by Eq. (80), namely

$$\mathbf{H}_3(x_3) = e^{\mathbf{F}_3 x_3} \left[\mathbf{M}_3 e^{\mathbf{F}_3 x_2} + \mathbf{N}_3 e^{\mathbf{F}_3 x_3} \right]^{-1}, \quad \boldsymbol{\gamma}_3 = \begin{Bmatrix} \mathbf{D}(x_2) \\ \mathbf{F} \end{Bmatrix}. \quad (122)$$

Expanding Eq. (121) yields

$$\begin{Bmatrix} \mathbf{D}(x_3) \\ \mathbf{D}'_3(x_3) \end{Bmatrix} = \begin{bmatrix} \mathbf{H}_{aa}^3(x_3) & \mathbf{H}_{ab}^3(x_3) \\ \mathbf{H}_{ba}^3(x_3) & \mathbf{H}_{bb}^3(x_3) \end{bmatrix} \begin{Bmatrix} \mathbf{D}(x_2) \\ \mathbf{F} \end{Bmatrix} \quad (123)$$

leading to the following generalized displacements at the tip of the beam:

$$\mathbf{D}(L) = \mathbf{H}_{aa}^3(x_3) \mathbf{D}(x_2) + \mathbf{H}_{ab}^3(x_3) \mathbf{F} \quad (124)$$

where $\mathbf{D}(x_2)$ is obtained from Eq. (111) for SC sensing and Eq. (117) for OC sensing.

3.2 Voltage/charge actuation

Here, a non-mechanically loaded ($\mathbf{F} = \mathbf{0}$) adaptive cantilever is considered for its voltage or charge actuation.

For the former, Eq. (95) reduces to

$$\begin{bmatrix} \mathbf{K}_{11}^{SC} & \mathbf{K}_{12}^{SC} \\ \mathbf{K}_{21}^{SC} & \mathbf{K}_{22}^{SC} \end{bmatrix} \begin{Bmatrix} \mathbf{D}(x_1) \\ \mathbf{D}(x_2) \end{Bmatrix} = \begin{Bmatrix} \tilde{\mathbf{V}} \\ -\tilde{\mathbf{V}} \end{Bmatrix} \quad (125)$$

where the voltage vector $\tilde{\mathbf{V}}$ is given by Eq. (82).

Following an identical procedure as in Eqs. (121) to (124), the generalized tip displacement vector of the beam is given by

$$\mathbf{D}(L) = \mathbf{H}_{aa}^3(x_3) \mathbf{D}(x_2) \quad (126)$$

with $\mathbf{D}(x_2)$ being obtained by solving Eq. (125).

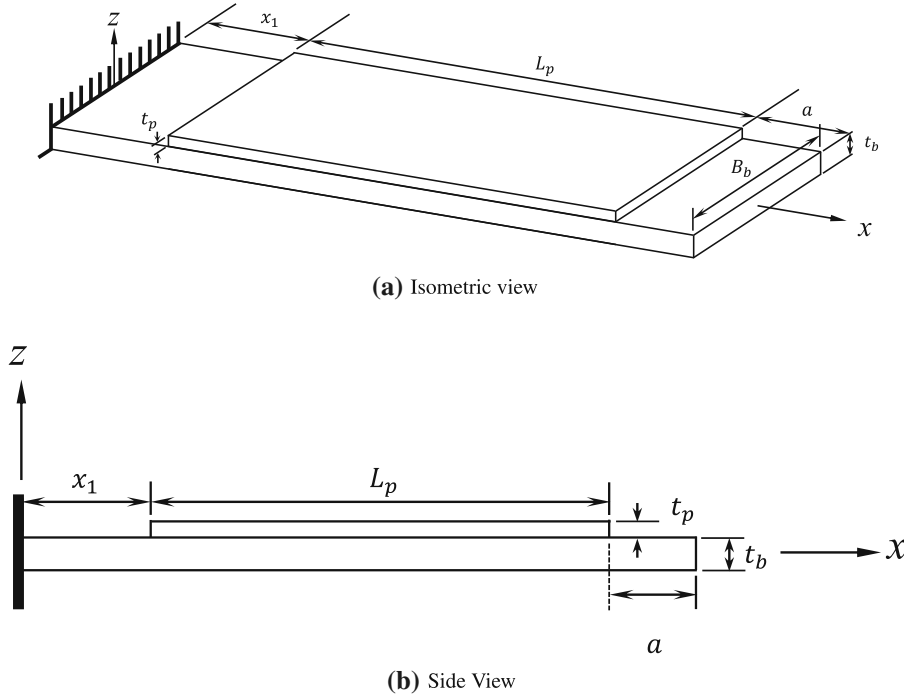


Fig. 2 A cantilever beam with a top surface-mounted piezoelectric patch

For the case of charge actuation, the corresponding generalized displacements $\mathbf{D}(x_1)$ and $\mathbf{D}(x_2)$ are obtained directly from Eq. (107) by setting $\mathbf{F} = \mathbf{0}$, so that

$$\begin{Bmatrix} \mathbf{D}(x_1) \\ \mathbf{D}(x_2) \end{Bmatrix} = \begin{bmatrix} \mathbf{K}_{11}^{OC} & \mathbf{K}_{12}^{OC} \\ \mathbf{K}_{21}^{OC} & \mathbf{K}_{22}^{OC} \end{bmatrix}^{-1} \begin{Bmatrix} \tilde{\mathbf{Q}} \\ -\tilde{\mathbf{Q}} \end{Bmatrix}. \quad (127)$$

Here, the generalized displacements at the tip of the beam, $\mathbf{D}(L)$, can be obtained using Eq. (126) with $\mathbf{D}(x_2)$ given by Eq. (127).

4 Numerical validation and benchmarking

The DTF CFS for static sensing/actuation of piezoelectric beam cantilevers have been implemented in MATLAB[®]. The latter's results are the induced potential/charge due to the static tip force, as solutions of the SC and OC sensing problems, and the tip generalized displacements as the solutions of the static voltage/charge actuation problems. In all benchmarks, the piezoelectric layers/patches are grounded at the interfaces with the host beam. The DTF solutions are validated by benchmarks that reported tabulated results [10–12, 14] or analytical formulas [13], as comparison to graphical results may lead to unwanted deviations. Therefore, limited benchmarks, namely patched asymmetric smart-beam [12], as in Fig. 2, unimorph [10, 11], as in Fig. 3, and trimorph [13, 14] as in Fig. 4, were found and used for validating and benchmarking the present DTF CFS.

4.1 Static sensing problems validation

One SC sensing (Fig. 3) and two OC sensing (Figs. 2 and 3) benchmarks are here analyzed. The piezoelectric layer/patch and host beam in these benchmarks have equal width as the host structure, and the corresponding material properties are recalled hereafter from [11, 12]. The static charge (SC) and voltage (OC) sensing results are obtained for an applied tip force, F_z , of $1 \mu\text{N}$.

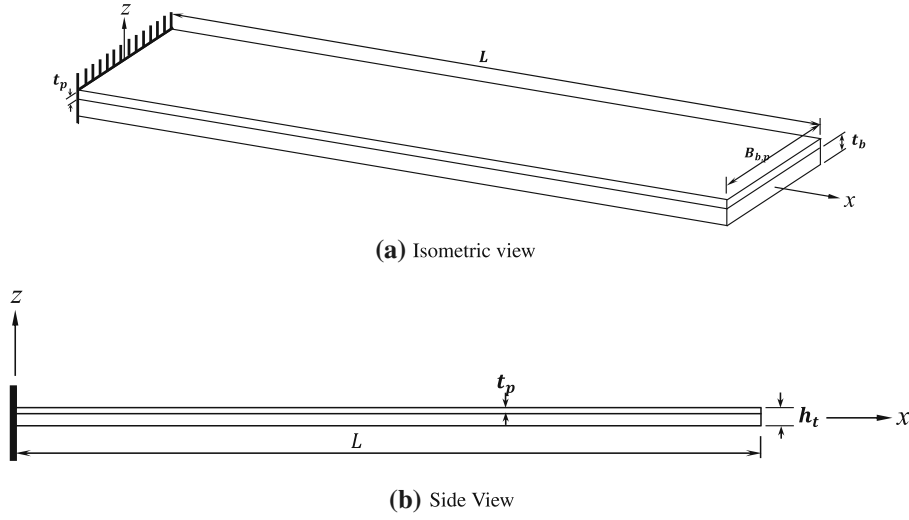


Fig. 3 Schematic diagram of a cantilever beam with a top surface-mounted piezoelectric layer (unimorph)

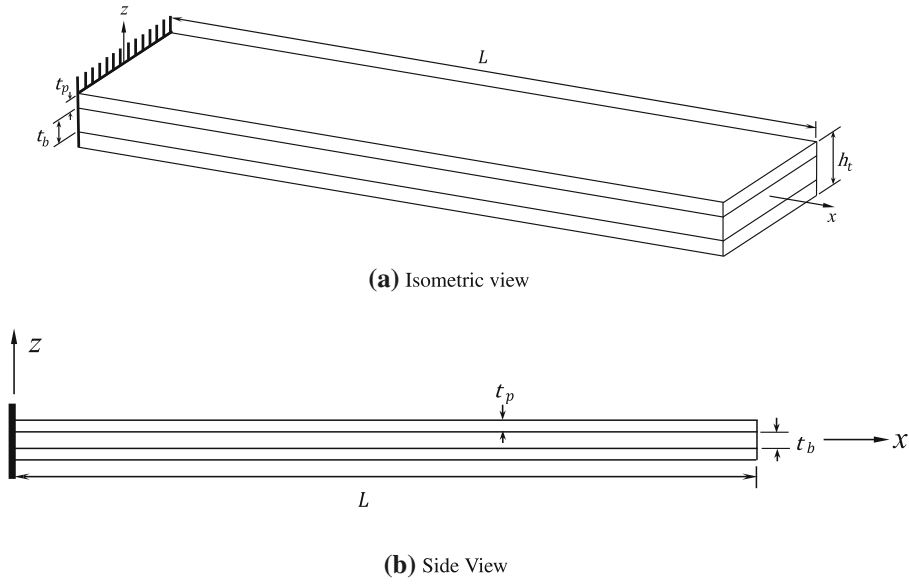


Fig. 4 Schematic diagram of a cantilever beam with surface-mounted piezoelectric layers (trimorph)

4.1.1 Short-circuit sensing

The proposed DTF CFS is compared to results from [11] obtained for the unimorph in Fig. 3. The latter has a length L of $1000 \mu\text{m}$ and a total thickness h_t of $6 \mu\text{m}$. The host beam, of thickness $t_b = \eta h_t$, is fully covered with an equal width, $B_p = B_b = 100 \mu\text{m}$, PZT-5A piezoceramic layer of thickness $t_p^u = (1 - \eta)h_t$. It is made from poly-silicon with a Young's modulus of 160 GPa and a Poisson's ratio of 0.2 . The used PZT-5A elastic stiffness coefficients at constant electric field are $C_{11}^E = 120.32 \text{ GPa}$, $C_{13}^E = 75.06 \text{ GPa}$, $C_{33}^E = 110.84 \text{ GPa}$, and $C_{55}^E = 21.05 \text{ GPa}$, the stress piezoelectric coupling coefficients are $e_{31} = -5.35 \text{ C/m}^2$ and $e_{33} = 15.78 \text{ C/m}^2$, and the transverse permittivity at constant strain is $\epsilon_{33}^S = 7.31 \text{ nF/m}$ [11]. Using the reduction provided in [11], which is based on plate kinematics and accounts for thickness strain, the piezoelectric layer modified axial and shear stiffness coefficients are calculated as $\tilde{Q}_{11}^E = 69.49 \text{ GPa}$ and $\tilde{Q}_{55}^E = 21.05 \text{ GPa}$, respectively, while the modified stress piezoelectric and blocked dielectric coefficients are

$\tilde{e}_{31} = -16.04 \text{ C/m}^2$ and $\tilde{\epsilon}_{33}^S = 9.56 \text{ nF/m}$, respectively. The reduced axial and shear coefficients for the host beam are $Q_{11}^b = 166.67 \text{ GPa}$ and $Q_{55}^b = 66.67 \text{ GPa}$, respectively. Reference [11] provides tabulated results for a thickness ratio $\eta = 2/3$. Using Eqs. (112) and (114), the calculated induced charge is found as $-10.105 \times 10^{-12} \text{ C}$. This value is 1.08% of relative deviation with regard to the $9.997 \times 10^{-12} \text{ C}$ value obtained by [11] using the 2D plane strain ANSYS[®] 4-node PLANE13 element. The difference in sign is due to the difference of the polarization direction. Furthermore, the corresponding SC sensed tip displacement $w_o(L)$, calculated using Eqs. (111) and (124), is computed as $1.692 \mu\text{m}$. This value is of 0.12% deviation from the $1.69 \mu\text{m}$ value, which was also obtained in [11] using the ANSYS[®] 2D plane strain PLANE13 element.

4.1.2 Open-circuit sensing

A patched asymmetric smart beam [12] as in Fig. 2 is here considered as a first OC sensing benchmark. The base aluminum beam is 79 mm long and has a thickness of $t_b = 3.9 \text{ mm}$, Young's modulus of $E = 69 \text{ GPa}$, and Poisson's ratio of $\nu = 0.3$. The PZT PIC255 piezoceramic patch has a thickness of $t_p = 0.3 \text{ mm}$, a length of 50 mm, and is placed 18 mm from the fixed end. The host and piezoceramic patch are of equal width $B_p = B_b = 25 \text{ mm}$. The piezoelectric patch plane-stress reduced electromechanical properties were given in [12] as $\tilde{Q}_{11}^E = 69.18 \text{ GPa}$, $\tilde{Q}_{55}^E = 21 \text{ GPa}$, $\tilde{e}_{31} = -16.57 \text{ C/m}^2$, and $\tilde{\epsilon}_{33}^S = 9.52 \text{ nF/m}$. The reduced elastic coefficients of the host beam are $Q_{11}^b = 75.82 \text{ GPa}$ and $Q_{55}^b = 26.54 \text{ GPa}$. An OC sensed voltage of 3 V was mentioned in [12] that was obtained using a plate discrete-layer finite element fulfilling the EP constraints on the patch electrodes. Using Eqs. (118) and (120), an OC sensed voltage of 3.1 V is obtained. This represents a relative deviation of 3.33% from the above reference value of 3 V.

The second benchmark considered here is the same unimorph as in the SC sensing case. The OC sensed voltage, calculated using Eqs. (118) and (120), is equal to 0.0171 V. This value is 1.18% of relative deviation from the -0.0169 V reported in [11] using the 2D plane strain ANSYS[®] 4-node PLANE13 element. The difference in sign is due to the difference of the polarization direction. On the other hand, the corresponding tip displacement is obtained, using Eqs. (117) and (124), as $1.705 \mu\text{m}$. This value is identical to that ($1.705 \mu\text{m}$) given in [11] using the 3D ANSYS[®] 8-node SOLID5 element.

4.2 Static actuation problems validation

The voltage and charge actuation problems are validated here by four benchmarks, a unimorph [10] similar in given dimensions and properties, including the calculated modified ones, as that used in the SC sensing case of Fig. 3, and trimorphs [13, 14] similar to that shown in Fig. 4. The DTF CFS voltage actuation problem is validated using three benchmarks [10, 13, 14], while the DTF CFS charge actuation one is validated against the unimorph benchmark results in [10].

4.2.1 Voltage actuation

The transverse tip displacement caused by an applied electric voltage is obtained here using Eqs. (125) and (126). The first voltage actuation benchmark is the unimorph [10] used earlier for validating the SC sensing problem. It is actuated by a voltage of 1 V applied on the top surface of the piezoelectric layer, while the actuator-beam interface remains grounded. The corresponding calculated tip displacement value is $-10.0194 \mu\text{m}$, which is of 0.85% relative deviation from the $10.105 \mu\text{m}$ 2D plane strain analytical value, reported in [10]. Again, the difference in sign is due to the difference of the polarization direction.

The second voltage actuation benchmark is a trimorph [13] as that shown in Fig. 4. It is 100 mm long and made of 16-mm-thick aluminum host with two, 1-mm-thick, surface-mounted piezoceramic layers, all having a unit width. The beam elastic properties are $E = 70.3 \text{ GPa}$ and $\nu = 0.345$, while the elastic properties used for the PZT-5H at constant electric field are $C_{11}^E = 126 \text{ GPa}$, $C_{13}^E = 84.1 \text{ GPa}$, $C_{33}^E = 117 \text{ GPa}$, and $C_{55}^E = 23 \text{ GPa}$, the stress piezoelectric coupling coefficients are $e_{31} = -6.5 \text{ C/m}^2$ and $e_{33} = 23.3 \text{ C/m}^2$ [13], and the transverse permittivity at constant strain is $\epsilon_{33}^S = 13 \text{ nF/m}$ [15]. Using the electromechanical coefficients reduction in [13], which is similar to that presented here in Eqs. (4) and (6), the modified elastic axial and shear stiffness coefficients are calculated as $\tilde{Q}_{11}^E = 65.55 \text{ GPa}$ and $\tilde{Q}_{55}^E = 23 \text{ GPa}$, respectively, while the modified stress piezoelectric and blocked dielectric coefficients are $\tilde{e}_{31} = -23.25 \text{ C/m}^2$ and $\tilde{\epsilon}_{33}^S = 17.64 \text{ nF/m}$. The reduced elastic coefficients of the aluminum host are $Q_{11}^b = 79.46 \text{ GPa}$ and $Q_{55}^b = 26.02 \text{ GPa}$.

Using the analytical equations provided by [13], the tip deflection for an applied voltage of 10 V is equal to $-0.5382 \mu\text{m}$, which is identical ($-0.5382 \mu\text{m}$) to DTF CFS calculated using Eqs. (125) and (126).

The third voltage actuation benchmark [14] is a trimorph similar to that of the previous voltage actuation case (Fig. 4), but with different material properties and dimensions. It is 0.3 m long, with host beam thickness of 0.02 m and two 0.005-m-thick piezoelectric layers. The width for this benchmark was not given; however, since all layers have equal width, it is factored out. The host beam is made of steel with $E = 210 \text{ GPa}$ and $\nu = 0.3$, while the piezoelectric layers are made of PZT-4 which used elastic stiffness coefficients at constant electric field being $C_{11}^E = 139 \text{ GPa}$, $C_{13}^E = 74.3 \text{ GPa}$, $C_{33}^E = 113 \text{ GPa}$, and $C_{55}^E = 25.6 \text{ GPa}$, stress piezoelectric coupling coefficients are $e_{31} = -6.98 \text{ C/m}^2$ and $e_{33} = 13.84 \text{ C/m}^2$, and transverse permittivity at constant strain is $\epsilon_{33}^S = 5.47 \text{ nF/m}$ [14]. The corresponding modified elastic axial and shear stiffness coefficients calculated using Eq. (4) are $\tilde{Q}_{11}^E = 90.15 \text{ GPa}$ and $\tilde{Q}_{55}^E = 25.6 \text{ GPa}$, respectively. The modified stress piezoelectric and blocked dielectric coefficients using (6) are $\tilde{e}_{31} = -16.08 \text{ C/m}^2$ and $\tilde{\epsilon}_{33}^S = 7.165 \text{ nF/m}$. The reduced elastic coefficients of the steel host are $Q_{11}^b = 230.77 \text{ GPa}$ and $Q_{55}^b = 80.77 \text{ GPa}$. For an applied voltage of 10 V, the reported tip displacement in [14] is equal to 566.9 nm, while the tip displacement calculated using Eqs. (125) and (126) is equal to 609.95 nm with a relative deviation of 7.6%. When using the PZT-4 data from eFunda [16] ($C_{11}^E = 139 \text{ GPa}$, $C_{13}^E = 74.28 \text{ GPa}$, $C_{33}^E = 115.41 \text{ GPa}$, $C_{55}^E = 25.6 \text{ GPa}$, $e_{31} = -5.203 \text{ C/m}^2$, $e_{33} = 15.08 \text{ C/m}^2$, and $\epsilon_{33}^S = 5.872 \text{ nF/m}$), the reduced electromechanical coefficients, according to Eqs. (4) and (6), are $\tilde{Q}_{11}^E = 91.19 \text{ GPa}$, $\tilde{Q}_{55}^E = 25.64 \text{ GPa}$, $\tilde{e}_{31} = -14.91 \text{ C/m}^2$ and $\tilde{\epsilon}_{33}^S = 7.84 \text{ nF/m}$, and the corresponding calculated tip displacement is 562.4 nm (compared to above 566.9 nm [14]) with a relative error of 0.75%.

4.2.2 Charge actuation

The charge-induced transverse tip displacement is obtained here using Eqs. (126) and (127). In the case of the unimorph (Fig. 3) used above in the validation of the voltage actuation problem [10] and for the thickness ratio $\eta = 2/3$, an electric charge of 6.5×10^{-10} Coulomb is applied to the top surface of the piezoelectric layer, while keeping the latter's interface with the beam grounded. Using the above equations, the current DTF CFS predicts a tip displacement of $11.04 \mu\text{m}$, which is of 0.01% deviation from the 2D plane strain, considering the so-called induced potential higher-order effect [8] analytical value ($11.039 \mu\text{m}$) reported in [10].

5 Conclusions and perspectives

Unified DTF CFS were presented for the static SC/OC sensing and voltage/charge actuation of beam cantilevers using top/bottom surface-mounted piezoelectric patches. These solutions can handle different material properties, thickness and width, but same length, for the patches. Besides, the latter's widths can be different from the host elastic beam as is usually the case in practice, but not in most literature theoretical (numerical or analytical) models. Therefore, the presented DTF CFS can handle unimorph and asymmetric or symmetric patched or layered smart cantilevers, but not bimorphs (two bonded piezoelectric layers only) and laminated hosts (the core layer of the trimorph). Another feature of the given solutions is that they can support various reduced piezoelectric constitutive equations and satisfy automatically the physical equipotential constraints on the piezoelectric patches/layers electrodes. The validation and benchmarking results showed very good correlations with the 2D plane-strain analytical [10] and 2D plane-strain [11, 14]/plane-stress [12, 13]/3D [11] finite element reference ones.

As a short-term perspective, the present work and earlier ones [6, 7] can be extended to laminated and piezoelectric hosts so that the above-mentioned layered composite host and bimorph limitations can be alleviated. Also, considering higher-order electric potential distributions through the thicknesses of the patches/layers will help gain higher accuracy. Next, as a mid-term perspective, a worthy extension could be directed to considering the case of embedded shear (d_{15}) piezoceramic sensors and actuators; corresponding SC and OC free-vibration solutions can be also investigated in order to assess the resulting dynamic electromechanical coupling. Finally, the extensions to multi-segments can be sought as a long-term perspective. This can alleviate, in particular, the above-mentioned patches same length limitation.

Compliance with ethical standards

Conflict of interest The authors declare that they have no conflict of interest.

Appendix: List of abbreviations

The following list of abbreviations has been introduced at their first appearance in the text and then used through this document:

1D	One-dimensional
2D	Two-dimensional
3D	Three-dimensional
BC	Boundary condition
CC	Continuity conditions
CFS	Closed-form solutions
DTF	Distributed transfer functions
EP	Equipotential
FEM	Finite element methods
FSDT	First-order shear deformation theory
OC	Open circuit
PDE	Partial differential equation
PVW	Principle of virtual work
SC	Short circuit
SSM	State space methods

References

1. Safaei, M., Sodano, H.A., Anton, S.R.: A review of energy harvesting using piezoelectric materials: state-of-the-art a decade later (2008–2018). *Smart Mater. Struct.* **28**(11), 113001 (2019)
2. Marakakis, K., Tairidis, G.K., Koutsianitis, P., Stavroulakis, G.E.: Shunt piezoelectric systems for noise and vibration control: a review. *Front. Built Environ.* **5**, 64 (2019). <https://doi.org/10.3389/fbuil.2019.00064>
3. Hajianmaleki, M., Qatu, M.S.: Vibrations of straight and curved composite beams: a review. *Compos. Struct.* **100**, 218–232 (2013)
4. Luschi, L., Iannaccone, G., Pieri, F.: A critical review of reduced one-dimensional beam models of piezoelectric composite beams. *J. Intell. Mater. Syst. Struct.* **30**(8), 1148–1162 (2019)
5. Yang, B., Tan, C.A.: Transfer functions of one-dimensional distributed parameter systems. *J. Appl. Mech.* **59**(4), 1009–1014 (1992)
6. Majeed, M.A., Al-Ajmi, M., Benjeddou, A.: Semi-analytical free-vibration analysis of piezoelectric adaptive beams using the distributed transfer function approach. *Struct. Control Health Monitor.* **18**(7), 723–736 (2011)
7. Majeed, M.A., Benjeddou, A., Al-Ajmi, M.: Free vibration analysis of moderately thick asymmetric piezoelectric adaptive cantilever beams using the distributed transfer function approach. *J. Sound Vib.* **333**(15), 3339–3355 (2014)
8. Benjeddou, A., Trindade, M.A., Ohayon, R.: A unified beam finite element model for extension and shear piezoelectric actuation mechanisms. *J. Intell. Mater. Syst. Struct.* **8**(12), 1012–1025 (1997)
9. Benjeddou, A.: Advances in piezoelectric finite element modeling of adaptive structural elements: a survey. *Comput. Struct.* **76**(1), 347–363 (2000)
10. Elka, E., Elata, D., Abramovich, H.: The electromechanical response of multilayered piezoelectric structures. *J. Microelectromech. Syst.* **13**(2), 332–341 (2004)
11. Elka, E., Elata, D., Abramovich, H.: The electromechanical response of multi-layered piezoelectric structures. *Tech. Rep. TME Report No. 478* (2003)
12. Al-Ajmi, M., Benjeddou, A.: A new discrete-layer finite element for electromechanically coupled analyses of piezoelectric adaptive composite structures. *Comput. Mater. Continua* **23**(3), 265–286 (2011)
13. Zhang, X.D., Sun, C.T.: Formulation of an adaptive sandwich beam. *Smart Mater. Struct.* **5**(6), 814–823 (1996)
14. Lau, C., Lim, C.W., Xu, R., Yu, Y., Yang, Q.: Behavior of a 3-layered thick piezoelectric actuator using a 2-D coupled electromechanical model. *Mech. Adv. Mater. Struct.* **16**(2), 120–129 (2009)
15. Sulbhevar, L.N., Raveendranath, P.: A consistently efficient and accurate higher order shear deformation theory based finite element to model extension mode piezoelectric smart beams. *J. Intell. Mater. Syst. Struct.* **27**(9), 1231–1249 (2016)
16. eFunda Inc: eFunda: properties of piezo material lead zirconate titanate (PZT-4). https://www.efunda.com/materials/piezo/material_data/matdata_output.cfm?Material_ID=PZT-4 Accessed: 2020-03-30 (2020)